Fully Spin-Transparent Magnetic Interfaces Enabled by the Insertion of a Thin Paramagnetic NiO Layer

Lijun Zhu, Lujun Zhu, and Robert A. Buhrman

Phys. Rev. Lett. **126**, 107204 — Published 12 March 2021

DOI: 10.1103/PhysRevLett.126.107204

Fully spin-transparent magnetic interfaces enabled by insertion of a thin paramagnetic NiO layer

Lijun Zhu[1,2*], Lujun Zhu[2], and Robert A. Buhrman[1]

1. Cornell University, Ithaca, New York 14850, USA

2. State Key Laboratory of Superlattices and Microstructures, Institute of Semiconductors, Chinese Academy of Sciences, P.O. Box 912, Beijing 100083, China

3. College of Physics and Information Technology, Shaanxi Normal University, Xi'an 710062, China

Spin backflow and spin-memory loss have been well established to considerably lower the interfacial spin transmissivity of metallic magnetic interfaces and thus the energy efficiency of spin-orbit torque technologies. Here we report that spin backflow and spin-memory loss at Pt-based heavy metal/ferromagnet interfaces can be effectively eliminated by inserting an insulating paramagnetic NiO layer of optimum thickness. The latter enables the thermal magnon-mediated essentially unity spin-current transmission at room temperature due to considerably enhanced effective spin-mixing conductance of the interface. As a result, we obtain dampinglike spin-orbit torque efficiency per unit current density of up to 0.8 as detected by the standard technology ferromagnet FeCoB and others, which reaches the expected upper-limit spin Hall ratio of Pt. We establish that Pt/NiO and Pt-Hf/NiO are two energy-efficient, integration-friendly, and high-endurance spin-current generators that provide >100 times greater energy efficiency than sputter-deposited topological insulators BiSb and BiSe. Our finding will benefit spin-orbitronic research and advance spin-torque technologies.

Spin-orbit torques (SOTs)[1-2] have great potential for enabling ultrafast energy-efficient magnetic memories [3,4] and logic [5] for many key electronics applications (e.g. large-scale computing and machine learning). However, energy-efficient, integration-friendly, and high-endurance spin-current generators, the indispensable basis for a successful SOT technology, have remained a major challenge after a decade of intensive exploration. The topological insulators BiSb [6,7] and BiSe [8], despite their high spin Hall ratios (θ_{SH}), are problematic because of their giant resistivities (ρ_{xx})[7,8] and poor thermal and chemical stabilities [9,10]. While some Pt-based heavy metals (HMs) with giant intrinsic spin Hall conductivity (σ_{SH}) and low ρ_{xx} [11-15] are integration-friendly high-endurance spin current generators, their energy-efficiency is lowered *considerably* by spin backflow (SBF) and sometime also by spin memory loss (SML) at the HM/ferromagnet (FM) interfaces [16-24].

As schematically shown in Fig. 1(a), the spin current generated by the spin Hall effect (SHE) of the HM drops sharply at the metallic HM/FM interface because of the degradation of the interfacial spin transparency (T_{int}) by SBF [16-18] and SML [19-24]. In the case of Pt-based HM/FM interfaces, the drift-diffusion analysis [16-18] indicates that SBF reduces T_{int}, thus the dampinglike SOT efficiency per applied electric field $\xi^E_{DL} \equiv (2e/\hbar)T_{int}\sigma_{SH}$ and dampinglike SOT efficiency per unit current density $\xi^j_{DL} \equiv T_{int}\theta_{SH}$ by more than a factor of 2 [12,15], while further reduction of T_{int} by SML will occur when the interfacial spin-orbit coupling (ISOC) is significant (e.g. at annealed Pt/Co interfaces)[20,22-24]. Consequently, the optimized Pt-based elemental film [11,12,20], alloys [12], and multilayers [15] that can have giant θ_{SH} of up to ≈ 0.6-0.8 only provide ξ^j_{DL} of <0.4 (ξ^j_{DL} = 0.16-0.22 for pure Pt [11-13]). While SML can be reduced by interface engineering (e.g. by interface alloying [25] or by insertion of an ultrathin passivating layer [20]), substantial SBF is inevitable at a metallic HM/FM interface when conduction electrons transport the spin angular momentum. So far, there has been no report on unity T_{int}, or equivalently $\xi^j_{DL} = \theta_{SH}$, in a Pt-based HM/FM system.

Recently, it has been established that spin current is transmittable in insulating NiO layers [26-31], providing an alternative, electron-free scheme for spin transport. However, both the mechanism and efficiency of the spin transport in NiO have remained in dispute. While some works argue that spin transport in NiO is mediated by coherent antiferromagnetic (AF) magnons [26,28,31] or by tunneling electrons [31], others suggest that the carriers of spin current can only be short-range thermal magnons [27,29]. The insertion of a thin NiO layer between a source and a detector of spin current has also been reported to significantly enhance [26,27,29,30], to abruptly suppress [31], or to have no effect on the spin transmission [28]. Notably, none of the previous experiments [26-31] has evaluated the values of T_{int} of NiO interfaces, and none of the inverse SHE experiments [26,27,29] has discussed the values of $T_{int}\theta_{SH}$ of their yttrium iron garnet (YIG)/NiO/HM samples. For SOT technologies [3-5], exerting a strong SOT on metallic FeCoB is more relevant and more important than increasing the inverse SHE voltage of insulating YIG/HM [26,29]. So far, the only report on enhancement of ξ^j_{DL} by NiO insertion is for Pt/CoTb [30], but the optimized ξ^j_{DL} in that work was below 0.09.

In this Letter, from direct SOT studies based on different techniques and material series, we, for the first time, identify that in a SOT process both SBF and SML at a metallic magnetic interface can be effectively eliminated at room temperature by the insertion of a thin paramagnetic NiO layer of optimum thickness (t_{NiO}~0.9 nm). The latter enables thermal magnon-mediated essentially unity spin-current transmission from the HM to the FM [Fig. 1(b)]. As a result, we obtained ξ^j_{DL} of up to 0.8, which is the expected upper-limit θ_{SH} of Pt [15].

For this study, we sputter-deposited two in-plane magnetized sample series: Pt 4/NiO 0-2.7/FeCoB 1.4 and Pt-Hf/NiO 0-2.7/FeCoB 1.4. Here, the numbers are the layer thicknesses in nm, FeCoB = $Fe_{60}Co_{20}B_{20}$, Pt-Hf = [Pt 0.6/Hf

$0.2]_5$/Pt 0.6. More details on the samples and experimental methods can be found in the Supplementary Materials [32]. The NiO layers are insulating (ρ_{xx} >10^7 μΩ cm), of disordered polycrystalline face-centered cubic structure (Fig. S1 in [32]), and paramagnetic at room temperature. The minimal exchange bias field (H_{EB}) and enhanced coercivity (H_c) at room temperature (Figs. 2(a)-2(c) and Fig. S9 in [32]) suggest that the Neél temperature (T_N) and the blocking temperature (T_B) are well below 300 K in the studied t_{NiO} range (T_N is close to and usually only slightly higher than T_B [29]). This is because FM/AF exchange coupling should occur below T_B and lead to non-zero H_{EB} and enhanced H_c. As indicated by the temperature dependences of H_{EB} and H_c in Figs. 2(a)-2(c), T_B for our 0.9 nm NiO is ≈125 K, which is lower than 170 K in [29] but much higher than 15 K in [31] for similar t_{NiO}.

The dampinglike SOT efficiencies are determined by angle-dependent "in-plane" harmonic Hall response measurement [12,39]. In the macrospin approximation, the second harmonic Hall voltage response ($V_{2\omega}$) to SOTs under an in-plane magnetic field (H_{in}) is given by $V_{2\omega} = V_a\cos\varphi + V_p\cos\varphi\cos2\varphi$ [12,39], where φ is the angle of H_{in} with respect to the current direction, $V_a = -V_{AH}H_{DL}/2(H_{in}+H_k)+V_{ANE}$, V_p is the contribution from the fieldlike SOT and the Oersted field, V_{AH} is the anomalous Hall voltage, V_{ANE} the anomalous Nernst effect due to the vertical thermal gradient, H_k the perpendicular anisotropy field, and H_{DL} the dampinglike SOT field. We determine the values of V_{AH} and H_k from the dependence of the first harmonic response Hall voltage ($V_{1\omega}$) on the swept out-of-plane field (H_z) under zero H_{in} (see Fig. 2(d) and Fig. S2 in [32]). We obtain V_a for each magnitude of H_{in} from the φ dependence of $V_{2\omega}$ [Fig. 2(e)]. The slopes and the intercepts of the linear fits of V_a vs $V_{AH}/2(H_{in}+H_k)$ give the values of H_{DL} and V_{ANE}, respectively [Fig. 2(f)]. We note that separation of the V_{ANE} term from the $-V_{AH}H_{DL}/2(H_{in}+H_k)$ term by performing φ-dependent measurement is critical for a correct estimation of SOTs (i.e. H_{DL} and $\xi_{DL}^{E(j)}$)[12,39]. $\xi_{DL}^{E(j)}$ of the samples can be determined following [14]

$$\xi_{DL}^{E} = \mu_0 H_{DL} M_s t_{CoPt}/E, \quad (1)$$

$$\xi_{DL}^{j} = (2e/\hbar)\mu_0 H_{DL} M_s t_{CoPt}/j_c, \quad (2)$$

where the charge current density $j_c = E\sigma_{xx}$. For our measurements, the applied electric field is $E \approx 66.7$ kV/m; the conductivity σ_{xx} varies from 2.3×10^6 to 3.2×10^6 Ω^{-1} m^{-1} for the Pt layers and from 0.71×10^6 to 0.91×10^6 Ω^{-1} m^{-1} for the Pt-Hf layer; $M_s \approx$ 1100-1400 emu/cm^3 is the effective magnetization of the FeCoB layer that incudes any magnetic dead layer and magnetic proximity effect (Fig. S2 in [32]).

As summarized in Figs. 2(g) and 2(h), in the absence of a NiO insertion layer, $\xi_{DL}^{E} \approx 4.8\times10^5$ Ω^{-1} m^{-1} ($\xi_{DL}^{j} \approx 0.18$) for Pt 4/FeCoB 1.4 and $\xi_{DL}^{E} \approx 3.5\times10^5$ Ω^{-1} m^{-1} ($\xi_{DL}^{j} \approx 0.37$) for Pt-Hf/FeCoB 1.4, which agree with previous reports [11-13,40]. As t_{NiO} increases, ξ_{DL}^{E} for each of the Pt/NiO/FeCoB and Pt-Hf/NiO/FeCoB series first increases rapidly towards a maximum value at $t_{NiO} \approx 0.9$ nm and then drops down to negligibly small value at $t_{NiO} = 2.7$ nm. ξ_{DL}^{j} ($= \xi_{DL}^{E}/\sigma_{xx}$) is also maximized at $t_{NiO} \approx 0.9$ nm because there is only a weak variation of σ_{xx} with insertion of the NiO. The threefold (twofold) enhancement of ξ_{DL}^{E} for Pt/NiO/FM (Pt-Hf/NiO/FM) is also confirmed by spin-torque ferromagnetic resonance measurements [32].

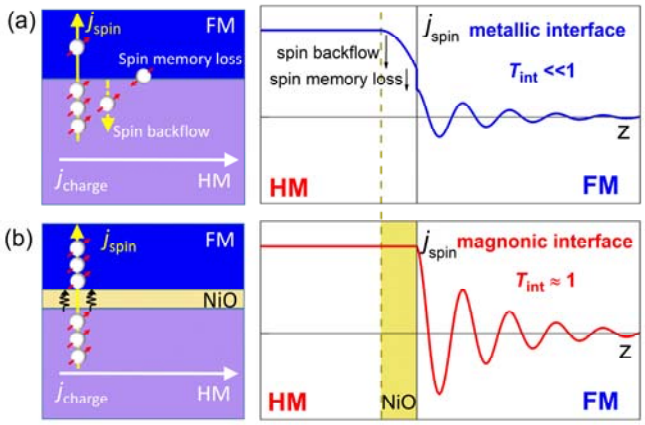

Fig. 1. (a) Metallic HM/FM interface where electron-mediated spin current diffuses from the HM to the FM and undergoes substantial SBF and SML (T_{int}<<1); (b) Magnonic HM/NiO/FM interface where thermal magnon-mediated spin transport is free of SBF and SML (T_{int}≈1) at the optimized thickness of the paramagnetic NiO. Here, the spin current flows perpendicular to the layers with spins pointing perpendicular to the magnetization. In the FM the spin current oscillates due to the rapid precession of the spin component that is transverse to the magnetization [16].

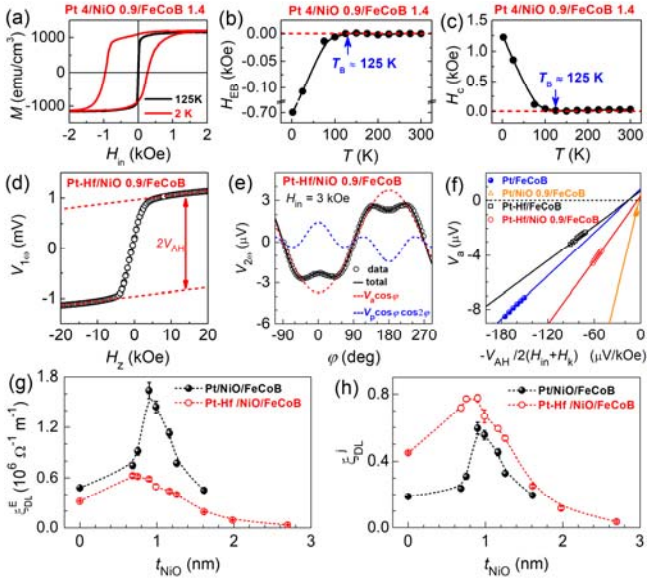

Fig. 2. (a) Magnetization hysteresis of Pt 4/NiO 0.9/FeCoB 1.4 at 2 K and 125 K. Temperature (T) dependence of (b) Exchange bias field and (c) Coercivity of the Pt 4/NiO 0.9/FeCoB 1.4, indicating a blocking temperature of ≈ 125 K for the 0.9 nm NiO layer. (d) First harmonic Hall voltage response ($V_{1\omega}$) vs H_z, (e) Second harmonic Hall voltage response ($V_{2\omega}$) vs φ (H_{in} = 3 kOe), (f) Linear dependence of V_a on $-V_{AH}/2(H_{in}+H_k)$ (H_{in} = 1.5-3.25 kOe), with the slopes

being H_{DL}, (g) ξ^E_{DL} and (h) ξ^j_{DL} for the HM/NiO t_{NiO}/FeCoB 1.4 (HM = Pt 4 or [Pt 0.6/Hf 0.2]$_5$/Pt 0.6) with different t_{NiO}.

This enhancement of the SOTs is not due to any spin current generation from the NiO layers, the NiO interfaces, or bulk effects in the FM since we measured a negligibly small ξ^E_{DL} for the control stack of Ta 1/NiO 0.9/FeCoB 1.4/Hf 0.1/MgO 2/Ta 1.5 (Fig. S4 in [32]). This first strongly suggests that the enhancement of ξ^E_{DL} in the HM/NiO/FeCoB is not due to a recently proposed mechanism [41] whereby a bi-axially anisotropic AF NiO single crystal can magnify (generate) spin current by spin angular momentum influx from the crystal lattice. This is likely because our sputter-deposited thin NiO layers are disordered and paramagnetic. The absence of any important interfacial Rashba-Edelstein effect in these samples is reaffirmed by the small fieldlike/dampinglike torque ratio (<0.1) [18] and the rapid decrease of both torques in the thick NiO limit (Fig. S5 in [32]). The minimal ξ^E_{DL} for another control stack of Pt 4/MgO 1.5/FeCoB suggests negligible spin current generation at the Pt/oxide interfaces of our samples. Therefore, the bulk SHE of Pt and Pt-Hf multilayers is the only important source for the dampinglike SOT in the Pt/NiO/FeCoB and Pt-Hf/NiO/FeCoB. As we discuss below, the dramatic evolution of ξ^E_{DL} with t_{NiO} for the HM/NiO/FM trilayer [Fig. 2(e)] is attributed to first the increase of T_{int} with t_{NiO} to essentially unity by the elimination of SBF, and then to a quasi-exponential decrease of T_{int} due to increasing spin attenuation within the NiO layer as t_{NiO} is beyond its optimal value.

It has been established that the dampinglike SOT in Pt-based alloys [12] and multilayers [15,40] is predominantly from the intrinsic SHE, with the signature being the characteristic reduction of σ_{SH} with carrier lifetime (or σ_{xx}) in the dirty limit [42]. Figure 3(a) shows the σ_{xx} dependence of the measured apparent spin Hall conductivity $T_{int}\sigma_{SH} = (\hbar/2e)\xi^E_{DL}$ and the estimated internal spin Hall conductivity $\sigma_{SH} = (\hbar/2e)\xi^E_{DL}/T_{int}$ for three different series of Pt-based materials: Pt-MgO alloys [12], Pt-Ti multilayers [15], and Pt-Hf multilayers [40]. In each case, both $T_{int}\sigma_{SH}$ and σ_{SH} decrease rapidly with decreasing σ_{xx} as expected for the intrinsic SHE in the dirty limit ($\sigma_{xx} < 4 \times 10^6$ Ω^{-1}-m^{-1})[42]. Our determination of T_{int} is discussed in detail in [32]. For these materials, SML is sufficiently weak so that the drift-diffusion analysis is approximately independent of SML ($T^{SML}_{int} > 0.9$ as determined from its linear dependence on ISOC [20]).

The rapid *increase* of ξ^E_{DL} in the region of $t_{NiO} < 0.9$ nm together with the unity T_{int} at $t_{NiO} \approx 0.9$ safely excludes the possibility of angular momentum transfer via electron tunneling through the insulating NiO layer. The latter, if important, would lead to a monotonic rapid decrease of ξ^E_{DL} with increasing t_{NiO} [26,27,29-31]. It has also been consistently found that insertion of a thin non-magnetic insulator layer (e.g. $SrTiO_3$ [26], AlO_x [29], SiO_2 [26,28], or MgO [30]) would degrade rather than enhance spin transmission, with a typical spin attenuation length (λ_s) of < 0.25 nm. Coherent AF magnons are apparently absent at room temperature in our HM/NiO/FM systems where the NiO is paramagnetic. This is reaffirmed by the very short λ_s of < 1 nm as indicated by the rapid, seemly exponential, decrease of ξ^E_{DL} (T_{int}) as t_{NiO} is increased above 0.9 nm. In sharp contrast, λ_s is very long (e.g. 5 nm [26,30] or >30 nm [31]) for coherent AF magnons in NiO layers that were prepared with different protocols and have large thicknesses and well-ordered crystal structures [26,28]. The *dc* spin current transmission in our paramagnetic NiO samples should be irreverent to coherent evanescent GHz spin waves that was argued to mediate *ac* spin current through epitaxial AF NiO (001)[43]. Therefore, short-range thermal magnons [29,44] are left as the only possible carriers for the highly efficient spin transport through our paramagnetic NiO. Note that the thermal magnons whose wavelength is shorter than the short-range spin correlation of the NiO remains above the T_N [29]. We find that this critical role of thermal magnons is suppressed at low temperatures where AF ordering of the NiO becomes increasingly restored (Section 9 in [32]), in consistence with the expectation that a large magnon band gap prohibits the excitation of thermal magnons and transmission of low-energy spin current [30,44].

Quantitatively, the absence of SBF at the optimal thickness of $t_{NiO} \approx 0.9$ nm suggest that magnonic spin-mixing conductance $G^{\uparrow\downarrow}_{eff,m}$ of the HM/NiO/FM composite interface is comparable to the Sharvin conductance of Pt (G_{Sh} =0.68×10^{15} Ω^{-1} m^{-2})[45], the upper bound of the effective spin-mixing conductance of a Pt interface [16,17], so that $T_{int} \approx 2G^{\uparrow\downarrow}_{eff,m}/G_{HM}$ reaches its limit of 1 (here the spin conductance (G_{HM}) is ≈ 1.3×10^{15} Ω^{-1} m^{-2}for Pt [46,47]). It is highly likely that the insertion of the thin insulating paramagnetic NiO blocks the less-efficient electron-mediated spin transport and enables short-range thermal magnon-mediated spin transport with a greatly enhanced $G^{\uparrow\downarrow}_{eff,m}$ [29,44]. Theoretical calculation of $G^{\uparrow\downarrow}_{eff,m}$ directly from the electronic, magnetic, and magnonic properties of the HM/NiO/FM system should be very informative, but is beyond the scope of this Letter.

Note that such impressive enhancement of T_{int} and SOTs we report in the Pt/NiO/FM and Pt-Hf/NiO/FM samples may not be necessarily expected for some other HM/NiO/FM systems. Apparently, T_{int} of those HM/FM samples with $G_{HM}/2 \leq G^{\uparrow\downarrow}_{eff,e}$ already reaches the limit of 1 and thus cannot be enhanced further by any NiO insertion. A good example is the Bi_2Se_3/NiO/$Ni_{81}Fe_{19}$ system [31] where Bi_2Se_3 has a very low spin conductance ($G_{BiSe} \approx 0.02 \times 10^{15}$ Ω^{-1} m^{-2} and $G^{\uparrow\downarrow}_{eff,e} \approx 0.60 \times 10^{15}$ Ω^{-1} m^{-2})[48]. More generally, $G^{\uparrow\downarrow}_{eff,m}$ should vary with t_{NiO} as well as with the types of the HM and the FM because it is determined collectively by the whole "composite" HM/NiO/FM interface rather than solely by the NiO layer. This conclusion is supported by a previous spin Seebeck/inverse SHE experiment [29] that the enhancement of the spin

transmission at YIG/NiO 1/HM compared to that of YIG/HM is strong when the HM is Pt but minimal when the HM is Pd or W. Furthermore, we find that $G^{\uparrow\downarrow}_{\mathrm{eff,m}}$ at a FM/NiO/Pt (or Pt-Hf) interface can be reduced to below $G^{\uparrow\downarrow}_{\mathrm{eff,e}}$ of the corresponding FM/Pt (or Pt-Hf) interface when the FM surface is oxidized and becomes a magnetically dead insulating layer that attenuates spin current (Section 8 in [32]). In addition, insertion of a very thick NiO layer that is AF at room temperature is not beneficial for T_{int} and $\xi^{E(j)}_{DL}$ [28,31] because the AF ordering will suppress excitation of thermal magnons and prohibit the transmission of low-energy spin current [30,44]. For example, insertion of a 25 nm AF NiO layer at $Bi_2Se_3/Ni_{81}Fe_{19}$ interface reduced ξ^{j}_{DL} from 0.67 to 0.3 [31], the latter is even smaller than that provided by some low-ρ_{xx} metals (e.g. Pt-Hf [40] and Pt-Ti multilayers [15]).

We also note that at interfaces of insulating YIG, where $G^{\uparrow\downarrow}_{\mathrm{eff,HM/YIG}}$ mediated only by thermal magnons in YIG [29] can be several times lower than $G^{\uparrow\downarrow}_{\mathrm{eff,e}}$ of metallic Pt/FM interfaces [46], a more than a factor of 3 *relative* increase of spin transmission by introducing the enhanced magnons of NiO is possible at the optimal temperatures [29,44]. While the lack of the $T_{\mathrm{int}}\theta_{\mathrm{SH}}$ values in previous YIG reports [26,27,29,44] prevents evaluation of the exact spin transparency of those YIG/NiO/HM, there is no doubt that the maximum T_{int} of any magnetic interfaces, in either a SOT process or an inverse SHE process, can never exceed unity and thus cannot be greater than that of our Pt (Pt-Hf)/NiO 0.9/FeCoB interfaces.

From the viewpoint of SOT technology, the fact that inserting a thin paramagnetic NiO of optimum thickness between a HM and a FM can result in effectively spin-transparent interfaces for spin transport from the HM to the FM is a very encouraging development. As shown in Fig. 2(f), with the insertion of 0.9 nm NiO layer, ξ^{j}_{DL} reaches 0.6 for 4 nm Pt (d = 4 nm, ρ_{xx}= 37 μΩ cm) and 0.8 for Pt-Hf multilayers (d = 4.6 nm, ρ_{xx}=132 μΩ cm). As compared in Figs. 3(b) and 3(c), this results in a SOT device energy efficiency (Section 10 and Table S2 in [32]) of >100 times higher than can be achieved with sputter-deposited β-W (d = 4 nm, ρ_{xx}=300 μΩ cm, ξ^{j}_{DL}= 0.3)[49], BiSb (d = 10 nm, ρ_{xx}=1000 μΩ cm, ξ^{j}_{DL}= 1.2)[7], BiSe (d = 4 nm, ρ_{xx}=13000 μΩ cm, ξ^{j}_{DL}= 18.6; d = 8 nm, ρ_{xx} = 2150 μΩ cm, ξ^{j}_{DL}= 2.88)[8]. [Note that a recent current-induced coercivity change measurement [6], which is a technique distinctly different from direct harmonic Hall response measurement, reported different results for *single-crystalline* BiSb (d = 10 nm, ρ_{xx} = 400 μΩ cm, ξ^{j}_{DL}= 52). While this would indicate a very low power consumption (6×10^{-5} times of that for the W device [49]), the single-crystalline BiSb requires molecular-beam epitaxy growth on single-crystalline GaAs(100)/MnGa(100)[6], making it disadvantageous for a practical technology that requires integration with CMOS circuits].

In addition to the power efficiency, the Pt/NiO/FM and Pt-Hf/NiO/FM systems are very promising for practical SOT technologies because their low resistivities are also critical for endurance and because of their CMOS integration-friendly properties. The latter includes thermal and chemical stability [20], compatibility with standard sputtering deposition on SiO_2 substrate, and ease of being combined with standard high-performance FeCoB magnetic tunnel junctions [4,40,50]. In contrast, BiSb and BiSe, despite their attractive values of ξ^{j}_{DL} [6-8], suffer from giant resistivities [7,8], thermal instabilities at even moderate temperatures (BiSb melts at 275 °C [9], BiSe sublimates at <280 °C [10]), and chemical instabilities in ambient atmosphere [9,10]. These aspects raise serious questions regarding both the endurance and power efficiency of any SOT devices based on these materials, and pose possibly insurmountable challenges for their successful integration with magnetic tunnel junctions and CMOS circuits. In contrast, Pt/NiO and Pt-Hf/NiO are two exceptionally impressive energy-efficient, integration-friendly, and high-endurance spin-current generators that should immediately benefit the development of practical SOT technologies and further stimulate spin-orbitronic research.

In conclusion, we have presented that SBF and SML at the Pt-based HM/FM interfaces, which considerably degrade the efficiencies of interfacial spin transport and dampinglike SOT, can be effectively eliminated by insertion of an insulating paramagnetic NiO layer of optimum thickness. We find that thermal magnons most likely mediate spin current in the HM/NiO/FM systems and considerably enhance the effective spin-mixing conductance ($G^{\uparrow\downarrow}_{\mathrm{eff,m}}$>>$G^{\uparrow\downarrow}_{\mathrm{eff,e}}$). The absence of SML is attributed to the negligible ISOC at the NiO/FM interface. We establish Pt/NiO (ρ_{xx}= 37 μΩ cm, ξ^{j}_{DL}=0.6) and Pt-Hf/NiO (ρ_{xx}= 132 μΩ cm, ξ^{j}_{DL}= 0.8) as two energy-efficient, integration-friendly, and high-endurance spin-current generators that provide >100 times greater energy efficiency than sputter-deposited BiSb and BiSe. Our finding will immediately benefit spin-orbitronic research and advance SOT technologies.

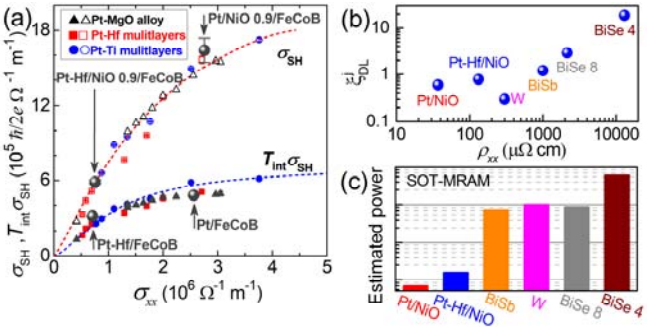

Fig. 3. (a) The variation of the internal (σ_{SH}) and apparent ($T_{\mathrm{int}}\sigma_{\mathrm{SH}}$) spin Hall conductivities with electrical conductivity of Pt-based systems. The solid (open) triangle, square, and circles represent $T_{\mathrm{int}}\sigma_{\mathrm{SH}}$ (σ_{SH}) of Pt-MgO alloys [12], Pt-Hf multilayers [40], and Pt-Ti multilayers [15], respectively. As indicated by the gray arrows, the four large gray solid dots

represent the $T_{int}\sigma_{SH}$ values directly measured for Pt-Hf/FeCoB, Pt-Hf/NiO 0.9/FeCoB, Pt/FeCoB, and Pt /NiO 0.9/FeCoB. While $T_{int}\sigma_{SH}$ for Pt/FeCoB and Pt-Hf/FeCoB overlaps with that for the electron-mediated Pt-MgO/Co, Pt-Hf/Co, and Pt-Ti/Co, $T_{int}\sigma_{SH}$ for the Pt/NiO 0.9/FeCoB and Pt-Hf/NiO 0.9/FeCoB matches the internal bulk values σ_{SH}, highlighting full spin transmission from the HM to FeCoB in the HM/NiO/FeCoB samples. The dashed lines are for guidance of eyes. (b) ξ_{DL}^{j} vs ρ_{xx} and (c) Estimated power for SOT-MRAM devices for the sputter-deposited Pt/NiO, Pt-Hf/NiO, BiSb [7], W [49], BiSe 8 nm, and BiSe 4 nm [8]. The power is normalized using that for the W device as unity.

The authors thank R. C. Tapping for instruction on oxide sputtering and Weiwei Lin for fruitful discussions on the spin transport in NiO. The authors acknowledge D. C. Ralph for a critical reading of the manuscript and very helpful suggestions. This work was supported in part by the Office of Naval Research (N00014-15-1-2449), in part by the NSF MRSEC program (DMR-1719875) through the Cornell Center for Materials Research, and in part by the NSF (ECCS-1542081) through use of the Cornell Nanofabrication Facility/National Nanotechnology Coordinated Infrastructure. The TEM measurements performed at Shaanxi Normal University were supported by the National Natural Science Foundation of China (Grant No. 51901121), the Science and Technology Program of Shaanxi Province (Grant No. 2019JQ-433), and the Fundamental Research Funds for the Central Universities (Grant No. GK201903024).

*lz442@cornell.edu

[1] I. M. Miron, K. Garello, G. Gaudin, P.-J. Zermatten, M. V. Costache, S. Auffret, S. Bandiera, B. Rodmacq, A. Schuhl, P. Gambardella, Nature 476, 189–193 (2011).
[2] L. Liu, C. F. Pai, Y. Li, H. W. Tseng, D. C. Ralph, R. A. Buhrman, Science 336, 555-558 (2012).
[3] E. Grimaldi, V. Krizakova, G. Sala, F. Yasin, S. Couet, G. S. Kar, K. Garello, P. Gambardella, Nat. Nanotech. 15, 111-117 (2020).
[4] L. Zhu, L. Zhu, S. Shi, D.C. Ralph, R.A. Buhrman, Adv. Electron. Mater. 6, 1901131 (2020).
[5] Z. Luo, A. Hrabec, T. P. Dao, G. Sala, S. Finizio, J. Feng, S. Mayr, J. Raabe, P. Gambardella, L. J. Heyderman, Nature 579, 214–218 (2020).
[6] N. H. D. Khang, Y. Ueda, P. N. Hai, Nat. Mater. 17, 808–813 (2018).
[7] Z. Chi, Y.-C. Lau, X. Xu, T. Ohkubo, K. Hono, M. Hayashi, Sci. Adv. 6, eaay2324 (2020).
[8] M. DC, R. Grassi, J.-Y. Chen, M. Jamali, D. R. Hickey, D. Zhang, Z. Zhao, H. Li, P. Quarterman, Y. Lv, M. Li, A. Manchon, K. A. Mkhoyan, T. Low, J.-P. Wang, Nat. Mater. 17, 800–807 (2018).
[9] C. Rochford, D. L. Medlin, K. J. Erickson, M. P. Siegal, APL Mater. 3, 126106 (2015).
[10] J. Buha, R. Gaspari, A. E. D. R. Castillo, F.Bonaccorso, L. Manna, Nano Lett. 16, 4217–4223 (2016).
[11] H. Wang, K.-Y. Meng, P. Zhang, J. T. Hou, J. Finley, J. Han, F. Yang, L. Liu, Appl. Phys. Lett. 2019, 114, 232406.
[12] L. Zhu, L. Zhu, M. Sui, D.C. Ralph, R.A. Buhrman, Sci. Adv. 5, eaav8025 (2019).
[13] K. Garello, I. M. Miron, C. O. Avci, F. Freimuth, Y. Mokrousov, S. Blügel, S. Auffret, O. Boulle, G. Gaudin, P. Gambardella, Nat. Nanotech. 8, 587–593 (2013).
[14] M.-H. Nguyen, D. C. Ralph, R. A. Buhrman, Phys. Rev. Lett. 116, 126601 (2016).
[15] L. Zhu, R. A. Buhrman, Phys. Rev. Appl. 12, 051002 (2019).
[16] P. M. Haney, H. W. Lee, K. J. Lee, A. Manchon, M. D. Stiles, Phys. Rev. B 87, 174411 (2013).
[17] Y.-T. Chen, S. Takahashi, H. Nakayama, M. Althammer, S. T. B. Goennenwein, E. Saitoh, and G. E. W. Bauer, Phys. Rev. B 87, 224401 (2013).
[18] V. P. Amin and M. D. Stiles, Phys. Rev. B **94**, 104420 (2016).
[19] J.-C. Rojas-Sánchez, N. Reyren, P. Laczkowski, W. Savero, J.-P. Attané, C. Deranlot, M. Jamet, J.-M. George, L. Vila, H. Jaffrès, Phys. Rev. Lett. 112, 106602 (2014).
[20] L. Zhu, D. C. Ralph, R. A. Buhrman, Phys. Rev. Lett. 122, 077201 (2019).
[21]Y. Liu, Z. Yuan, R. J. H. Wesselink, A. A. Starikov, P. J. Kelly, Phys. Rev. Lett. **113**, 207202 (2014).
[22] K. Chen and S. Zhang, Phys. Rev. Lett. **114**, 126602 (2015).
[23] J. Borge and I. V. Tokatly, Phys. Rev. B **96**, 115445 (2017).
[24] K. Dolui and B. K. Nikolić, Phys. Rev. B 96, 220403(R)(2017).
[25] L. Zhu, D. C. Ralph, R. A. Buhrman, Phys. Rev. B 99, 180404 (2019).
[26] H. L. Wang, C. H. Du, P. C. Hammel, F. Y. Yang, Phys. Rev. Lett. 113, 097202 (2014).
[27] C. Hahn, G. de Loubens, O. Klein, M. Viret, V. V. Naletov, J. B. Youssef, Europhys. Lett. 108, 57005 (2014).
[28] T. Moriyama, S. Takei, M. Nagata, Y. Yoshimura, N. Matsuzaki, T. Terashima, Y. Tserkovnyak, T. Ono, Appl. Phys. Lett. 106, 162406 (2015).
[29] W. Lin, K. Chen, S. Zhang, C. L. Chien, Phys. Rev. Lett. 116, 186601 (2016).
[30] H. Wang, J. Finley, P. Zhang, J. Han, J. T. Hou, L. Liu, Phys. Rev. Appl. 11, 044070 (2019).
[31] Y. Wang, D. Zhu, Y. Yang, K. Lee, R. Mishra, G. Go, S.-H. Oh, D.-H. Kim, K. Cai, E. Liu, S. D. Pollard, S. Shi, J. Lee, K. L. Teo, Y. Wu, K.-J. Lee, H. Yang, Science 366, 1125 (2019).
[32] see the Supplementary Materials for more information on sample preparation and characterization, spin-torque ferromagnetic resonance measurement of effect of NiO insertion, absence of significant spin-orbit torques from the interfaces, estimation of interfacial spin transparency, distinct dependences of spin transparency and magnetic damping on the NiO thickness, minimal interfacial spin-orbit coupling at NiO/FeCoB interface, absence of exchange

bias at room temperature, influence of potential interfacial oxidation, temperature dependence of spin-orbit torques in Pt 4/NiO 0.9/FeCoB 1.4, and calculation of power consumption of the SOT devices, which includes Ref. [33-38].

[33] C.-F. Pai, Y. Ou, L. H. Vilela-Leao, D. C. Ralph, R. A. Buhrman, Phys. Rev. B 92, 064426 (2015).
[34] L. Zhu, L. Zhu, D. C. Ralph, R. A. Buhrman, Phys. Rev. Appl. 13, 034038 (2020).
[35] C. Kittel, Phys. Rev. 73, 155 (1948).
[36] Y. Ou, C.-F. Pai, S. Shi, D. C. Ralph, and R. A. Buhrman, Phys. Rev. B 94, 140414(R) (2016).
[37] A. R. Mellnik, J. S. Lee, A. Richardella, J. L. Grab, P. J. Mintun, M. H. Fischer, A. Vaezi, A. Manchon, E.-A. Kim, N. Samarth, D. C. Ralph, Nature 511, 449–451 (2014).
[38] L. Zhu, D. C. Ralph, R. A. Buhrman, Phys. Rev. Appl. 10, 031001 (2018).
[39] C. O. Avci, K. Garello, M. Gabureac, A. Ghosh, A. Fuhrer, S. F. Alvarado, P. Gambardella, Phys. Rev. B 90, 224427 (2014).
[40] L. Zhu, L. Zhu, S. Shi, M. Sui, D.C. Ralph, R.A. Buhrman, Phys. Rev. Appl. 11, 061004 (2019).
[41] R. Khymyn, I. Lisenkov, V. S. Tiberkevich, A. N. Slavin, B. A. Ivanov, Phys. Rev. B 93, 224421 (2016).
[42] T. Tanaka, H. Kontani, M. Naito, T. Naito, D. S. Hirashima, K. Yamada, and J. Inoue, Phys. Rev. B 77, 165117 (2008).
[43] M. Dąbrowski, T. Nakano, D. M. Burn, A. Frisk, D. G. Newman, C. Klewe, Q. Li, M. Yang, P. Shafer, E. Arenholz, T. Hesjedal, G. van der Laan, Z.Q. Qiu, and R. J. Hicken, Phys. Rev. Lett. 124, 217201(2020).
[43] Z. Qiu, J. Li, D. Hou, E. Arenholz, A. T. N'Diaye, A. Tan, K. Uchida, K. Sato, S. Okamoto, Y. Tserkovnyak, Z. Q. Qiu, E. Saitoh, Nat. Commun. 7, 12670 (2016).
[45] M. Zwierzycki, Y. Tserkovnyak, P. Kelly, A. Brataas, and G. E. W. Bauer, Phys. Rev. B 71, 064420 (2005).
[46] L. Zhu, D. C. Ralph, R. A. Buhrman, Phys. Rev. Lett. 123, 057203 (2019).
[47] E. Sagasta, Y. Omori, M. Isasa, M. Gradhand, L. E. Hueso, Y. Niimi, Y. Otani, and F. Casanova, Phys. Rev. B 94, 060412(R)(2016).
[48] P. Deorani, J. Son, K. Banerjee, N. Koirala, M. Brahlek, S. Oh, and H. Yang, Phys. Rev. B 90, 094403 (2014).
[49] C. F. Pai, L. Liu, Y. Li, H. W. Tseng, D. C. Ralph, R. A. Buhrman, Appl. Phys. Lett. 101, 122404 (2012).
[50] S. V. Aradhya, G. E. Rowlands, J. Oh, D. C. Ralph, R. A. Buhrman, Nano Lett. 16, 5987–5992 (2016).